Characterizing invisible electroweak particles through single-photon processes at high energy e^+e^- colliders

Seong Youl Choi,[1,2] Tao Han,[2,3,4] Jan Kalinowski,[5] Krzysztof Rolbiecki,[5,6] and Xing Wang[2]

[1]*Department of Physics, Chonbuk National University, Jeonbuk 561-756, Korea*
[2]*Pittsburgh Particle Physics, Astrophysics, and Cosmology Center, Department of Physics and Astronomy, University of Pittsburgh, Pittsburgh, Pennsylvania 15260, USA*
[3]*Center for High Energy Physics, Tsinghua University, Beijing 100084, China*
[4]*Korea Institute for Advanced Study (KIAS), Seoul 130-012, Korea*
[5]*Faculty of Physics, University of Warsaw, 02093 Warsaw, Poland*
[6]*IFT-UAM/CSIC, C/ Nicolás Cabrera 13-15, 28049 Madrid, Spain*

(Received 7 April 2015; published 5 November 2015)

We explore the scenarios where the only accessible new states at the electroweak scale consist of a pair of color-singlet electroweak particles, the masses of which are degenerate at the tree level and split only by electroweak symmetry breaking at the loop level. For the sake of illustration, we consider a supersymmetric model and study the following three representative cases with the lower-lying states as (a) two spin-1/2 Higgsino $\mathrm{SU}(2)_L$ doublets, (b) a spin-1/2 wino $\mathrm{SU}(2)_L$ triplet and (c) a spin-0 left-handed slepton $\mathrm{SU}(2)_L$ doublet. Due to the mass degeneracy, those lower-lying electroweak states are difficult to observe at the LHC and rather challenging to detect at the e^+e^- collider as well. We exploit the pair production in association with a hard photon radiation in high energy e^+e^- collisions. If kinematically accessible, such single-photon processes at e^+e^- colliders with polarized beams enable us to characterize each scenario by measuring the energy of the associated hard photon and to determine the spin of the nearly invisible particles unambiguously through the threshold behavior in the photon energy distribution.

DOI: 10.1103/PhysRevD.92.095006 PACS numbers: 12.60.Jv, 12.60.Cn, 12.60.-i, 14.80.Ly

I. INTRODUCTION

The discovery of the Higgs boson at the CERN LHC [1,2] truly sets a milestone in particle physics. It completes the structure of the standard model (SM), which may be valid as a self-consistent effective theory all the way up to the Planck scale. The rather light mass of 125 GeV [3] and narrow width of much less than a GeV [4,5] for the Higgs boson imply a weakly coupled theory at work for the electroweak symmetry-breaking (EWSB) sector. The naturalness argument [6–9] thus prefers the existence of new states associated with the EWSB sector. Supersymmetry [10,11] is arguably the best motivated candidate for a natural theory, and the relevant partners include top squarks, gluinos, electroweak (EW) gauginos and Higgsinos. Another important feature of supersymmetric (SUSY) models is the lightest neutral SUSY particle to serve as a cold dark matter candidate [12,13]. However, it has been quite puzzling that, except for a SM-like Higgs boson, no new particles beyond the SM have been so far observed in the LHC experiments near and above the TeV threshold. One plausible scenario for the LHC null search results is that all the colored SUSY particles with QCD strong interactions are rather heavy and thus out of reach [14–19]. The EW particles, although kinematically accessible, may not lead to experimentally tractable signals due to the rather small production rate, the uncharacteristic signature and the large SM backgrounds at hadron colliders [17,20–35]. This situation happens quite naturally when the lower-lying EW states are nearly degenerate in mass, and thus the final-state products are rather soft and have little missing transverse energy. On the other hand, the future e^+e^- colliders, such as the International Linear Collider (ILC) [36–38], would be capable of covering the search as long as kinematically accessible, because of the well-constrained event topology and the very clean experimental environment.

In this paper, we set out to study this challenging scenario at an e^+e^- collider in a rather model-independent way, to quantify the observability for the missing particle signal, and to explore the feasibility to determine the missing particle spin and chiral couplings. Within a generic framework of the minimal supersymmetric standard model (MSSM), we focus on three representative cases to study the EW lower-lying states, where the other SUSY particles are assumed to be decoupled. The first scenario, to be called the spin-1/2 Higgsino scenario, is the case where the only accessible SUSY particles are two spin-1/2 Higgsino doublets ($\tilde{H}^+$, $\tilde{H}^0$). The second scenario, to be called the spin-1/2 wino scenario, is the case where the only accessible SUSY particles are a spin-1/2 wino triplet ($\tilde{W}^+$, $\tilde{W}^0$, $\tilde{W}^-$). The third scenario, to be called the spin-0 slepton scenario, is the case where the only accessible SUSY particles consist of a spin-0 left-handed slepton doublet ($\tilde{\nu}_\ell$, $\tilde{\ell}^-$).

In each scenario, the charged particle and its neutral partner are degenerate in mass before EWSB, and their mass splitting originates dominantly from loop-induced EWSB corrections in the Higgsino and wino scenarios, or from the so-called D-term potential after EWSB in the slepton scenario. Due to the near degeneracy, it would be very challenging to observe the soft final-state particles. Analogous to the monojet plus missing energy signature at hadron colliders [39,40], a single energetic photon plus missing energy at e^+e^- colliders is known to be one of the promising search channels for the missing particles [20,26,27,41,42]. This method was used for counting neutrino families [43–45], as a means to search for heavy neutrinos [46] or (nearly) invisible SUSY particles [47–56], or anomalous gauge couplings [57–59]. We provide systematic and detailed methods not only for determining the spins of the (nearly) invisible particles unambiguously but also for characterizing each of the three benchmark scenarios through single-photon processes at e^+e^- colliders by exploiting electron and positron beam polarizations. We find that, if kinematically accessible, the spins and coupling strengths of the invisible particles to γ/Z in such single-photon processes can be determined clearly by exploiting the initial electron (and positron) beam polarization and investigating the threshold excitation patterns of the processes.

The remainder of the paper is organized as follows. We first set up the three benchmark scenarios in the MSSM framework. We lay out their spectra and interactions with the SM particles. We present the mass splitting in each scenario by radiative corrections or by D-term. Section III is devoted to systematic analyses for the radiative processes involving the pair production and an associated hard photon in e^+e^- collisions with special emphasis on the comparison of the initial-state radiation (ISR) and final-state radiation (FSR) in the charged pair production. We present the dependence of the cross sections on the photon energy and the electron/positron beam polarizations. In Sec. IV, we first study the discovery limit of the new invisible particles based on the statistical significance of each mode at a 500 GeV ILC. We then describe systematically how the threshold behavior and the ratios of polarized cross sections enable us to determine the SUSY particle spin and characterize each scenario unambiguously. We briefly comment on the other alternative methods for characterizing the properties of the scenarios. Finally, we summarize our results and present our conclusions in Sec. V.

II. SCENARIOS WITH A DEGENERATE PAIR OF SUSY PARTICLES

To study the nearly degenerate EW states in a relatively model-independent way, we take the MSSM as a generic framework and make the following simple assumptions: only a pair of SUSY color-singlet EW particles is kinematically accessible below the ILC threshold, and the other heavier states are essentially decoupled. This could be realized when the soft SUSY-breaking scalar quark masses and the gluino mass scale M_3 are much heavier than the EW soft SUSY-breaking scales. Specifically, we consider three benchmark scenarios in MSSM, each representing a qualitatively different case, as described in detail below.

A. Spin-1/2 Higgsino ($H_{1/2}$) scenario

The first scenario for a degenerate pair of EW new states, the scenario $H_{1/2}$, is provided by the Higgsino sector with the spin-1/2 SUSY partners of the down- and up-type Higgs bosons in the MSSM. This is realized practically when the Higgsino mass parameter μ of the superpotential term $\mu\hat{H}_d\cdot\hat{H}_u$ mixing the two Higgs superfields is much smaller than all the other SUSY parameters including the gaugino mass parameters, $M_{1,2,3}$ [17,20,22–25,27]. (Without any loss of generality, we assume the parameters, $M_{1,2}$ and μ, to be real and positive in the present paper.) When the gaugino states as well as the other SUSY states are decoupled without generating any mixing with the Higgsinos, the two SU(2)-doublet Higgsino states $\tilde{H}_d = [\tilde{H}^0_{dL}, \tilde{H}^-_{dL}]$ and $\tilde{H}_u = [\tilde{H}^+_{uL}, \tilde{H}^0_{uL}]$ have maximal mixing. The mass term for the charged and neutral Higgsino states can be cast into the mass term for a degenerate pair of a Dirac chargino and a Dirac neutralino with mass μ as

$$\mu\left(\overline{\tilde{H}^-_{uR}}\tilde{H}^-_{dL} + \overline{\tilde{H}^+_{dR}}\tilde{H}^+_{uL}\right) - \mu\left(\overline{\tilde{H}^0_{uR}}\tilde{H}^0_{dL} + \overline{\tilde{H}^0_{dR}}\tilde{H}^0_{uL}\right) \Rightarrow \mu\overline{\chi^-_H}\chi^-_H + \mu\overline{\chi^0_H}\chi^0_H, \quad (1)$$

where the Dirac chargino and Dirac neutralino are defined by

$$\chi^-_H = \tilde{H}^-_{dL} + \tilde{H}^-_{uR} \quad \text{and} \quad \chi^0_H = \tilde{H}^0_{dL} - \tilde{H}^0_{uR} \quad (2)$$

in terms of the current Higgsino states with the charge-conjugated states, $\tilde{H}^-_{uR} = (\tilde{H}^+_{uL})^c$ and $\tilde{H}^0_{uR} = (\tilde{H}^0_{uL})^c$.

As the down- and up-type Higgsinos form a vectorlike $SU(2)_L$ doublet, the interactions of the Dirac chargino χ^-_H and Dirac neutralino χ^0_H with the electromagnetic (EM) and weak gauge bosons are described by the Lagrangian

$$\begin{aligned}\mathcal{L}^H_{V\chi\chi} = {} & e\overline{\chi^-_H}\gamma^\mu\chi^-_H A_\mu + e\frac{(1/2 - s_W^2)}{c_W s_W}\overline{\chi^-_H}\gamma^\mu\chi^-_H Z_\mu \\ & - \frac{1}{2}\frac{e}{c_W s_W}\overline{\chi^0_H}\gamma^\mu\chi^0_H Z_\mu \\ & - \frac{e}{\sqrt{2}s_W}(\overline{\chi^0_H}\gamma^\mu\chi^-_H W^+_\mu + \text{H.c.}),\end{aligned} \quad (3)$$

where the Lorentz structure of every gauge interaction term is of a pure vector type and its strength is fixed only by the positron electric charge e and weak mixing angle θ_W. In the present paper, we use the abbreviations $s_W = \sin\theta_W$ and $c_W = \cos\theta_W$ for the sake of convenience.

B. Spin-1/2 wino ($W_{1/2}$) scenario

The second scenario for a degenerate pair of SUSY states, the $W_{1/2}$ scenario, is provided by the MSSM wino sector with the spin-1/2 partners of the $SU(2)_L$ gauge bosons. This is realized practically when the $SU(2)_L$ gaugino mass parameter M_2 is much smaller than the other gaugino mass parameters $M_{1,3}$ and the Higgsino mass parameter μ as well as all the other SUSY parameters [22,23,28–32]. In this scenario the mass term of the SU(2)-triplet wino state $\tilde{W} = [\tilde{W}_L^+, \tilde{W}_L^0, \tilde{W}_L^-]$ can be cast into a Dirac mass term for a Dirac chargino and a Majorana mass term for a Majorana neutralino with a common mass M_2 as

$$M_2\left(\overline{\tilde{W}_R^+}\tilde{W}_L^+ + \overline{\tilde{W}_R^0}\tilde{W}_L^0 + \overline{\tilde{W}_R^-}\tilde{W}_L^-\right) \Rightarrow M_2\overline{\chi_W^-}\chi_W^- + \frac{1}{2}M_2\overline{\chi_W^0}\chi_W^0 \quad (4)$$

by defining a Dirac chargino χ_W^- and a Majorana neutralino χ_W^0 by

$$\chi_W^- = \tilde{W}_L^- + \tilde{W}_R^- \quad \text{and} \quad \chi_W^0 = \tilde{W}_L^0 + \tilde{W}_R^0 \quad (5)$$

with the charge-conjugated states $\tilde{W}_R^\pm = (\tilde{W}_L^\mp)^c$ and $\tilde{W}_R^0 = (\tilde{W}_L^0)^c$. Note that by definition the neutralino state is identical to its charge-conjugated antiparticle, i.e. $(\chi_W^0)^c = \chi_W^0$.

In the $W_{1/2}$ scenario, the interactions of the vectorlike SU(2)-triplet states with the EM and weak gauge bosons are described by

$$\mathcal{L}_{V\chi\chi}^W = e\overline{\chi_W^-}\gamma^\mu\chi_W^- A_\mu + e\frac{(1-s_W^2)}{c_W s_W}\overline{\chi_W^-}\gamma^\mu\chi_W^- Z_\mu - \frac{e}{s_W}(\overline{\chi_W^0}\gamma^\mu\chi_W^- W_\mu^+ + \text{H.c.}). \quad (6)$$

Again, like the $H_{1/2}$ scenario, the Lorentz structure of every gauge interaction term is of a pure vector type, but the coupling strengths determined uniquely by the weak mixing angle θ_W are characteristically different from those in the $H_{1/2}$ scenario. Note that the Majorana neutralino in the $W_{1/2}$ scenario couples neither to the photon nor to the neutral weak boson Z.

C. Left-handed slepton (L_0) scenario

The third scenario for a degenerate pair of SUSY states, the L_0 scenario, is provided by the MSSM left-handed slepton sector with the spin-0 partners $\tilde{L} = [\tilde{\nu}_\ell, \tilde{\ell}_L^-]$ of the $SU(2)_L$-doublet lepton. This is realized practically when the SUSY-breaking slepton mass parameter $\tilde{m}_{\ell_L}$ is much smaller than all the other SUSY parameters. In general, the charged slepton $\tilde{\ell}_L^-$ and the sneutrino $\tilde{\nu}_\ell$ are nondegenerate and split by the so-called D-term potential after EWSB $\Delta m^2 = m_{\tilde{\ell}_L^-}^2 - m_{\tilde{\nu}_\ell}^2 = -m_Z^2\cos 2\beta c_W^2$, vanishing for $\tan\beta = 1$. For the sake of comparison, the charged slepton and neutral sneutrino may be assumed to be degenerate with $\tan\beta = 1$ at the tree level.

In the L_0 scenario, the interactions of the left-handed SU(2)-doublet slepton state with the EM and weak gauge bosons are described by the Lagrangian

$$\mathcal{L}_{V\tilde{\ell}_L\tilde{\ell}_L}^L = e\tilde{\ell}_L^+\overleftrightarrow{\partial_\mu}\tilde{\ell}_L^- A^\mu + e\frac{(1/2-s_W^2)}{c_W s_W}\tilde{\ell}_L^+\overleftrightarrow{\partial_\mu}\tilde{\ell}_L^- Z^\mu - \frac{1}{2}\frac{e}{c_W s_W}\tilde{\nu}_\ell^*\overleftrightarrow{\partial_\mu}\tilde{\nu}_\ell Z^\mu - \frac{e}{\sqrt{2}s_W}(\tilde{\nu}_\ell^*\overleftrightarrow{\partial_\mu}\tilde{\ell}_L^- W^{+\mu} + \text{H.c.}), \quad (7)$$

where $A\overleftrightarrow{\partial_\mu}B = A\partial_\mu B - (\partial_\mu A)B$. Note that the gauge coupling strengths of the charged slepton and neutral sneutrino are identical to those of the Dirac chargino and Dirac neutralino in the Higgsino case. However, because of their zero spin values, the Lorentz structure of the gauge interactions is different from that of the chargino and neutralino states. In addition, there exist four-point contact gauge interactions of left-handed sleptons. The Lagrangian for the $\gamma\gamma\tilde{\ell}_L^-\tilde{\ell}_L^-$ and $\gamma Z\tilde{\ell}_L^-\tilde{\ell}_L^-$ four-point vertices reads

$$\mathcal{L}_{\gamma Z\tilde{\ell}_L^-\tilde{\ell}_L^-}^L = e^2\tilde{\ell}_L^+\tilde{\ell}_L^- A_\mu A^\mu + 2e^2\frac{(1/2-s_W^2)}{c_W s_W}\tilde{\ell}_L^+\tilde{\ell}_L^- A_\mu Z^\mu. \quad (8)$$

Because of these momentum-independent contact terms, the charged slepton pair production associated with a hard final-state as well as initial-state photon emission exhibits an S-wave threshold excitation pattern in contrast to the P-wave excitation pattern in the neutral sneutrino pair production only with a hard initial photon emission, as shown later in Sec. III B.

D. Feynman rules for a vector boson converting into a particle pair and a photon

Depending on the electric charge and spin of the SUSY EW particle X, the vertex $VX\bar{X}$ for the process $V^*(q) \to X(q_1)\bar{X}(q_2)$ with $V = \gamma, Z$ can be parametrized as

$$\langle X(q_1)\bar{X}(q_2)||V^\mu(q)\rangle = ec_X^V\begin{cases}(q_1-q_2)^\mu & \text{for spin-0 chaged sleptons or sneutrinos}\\ \bar{u}(q_1)\gamma^\mu v(q_2) & \text{for spin-1/2 chargino or neutralinos}\end{cases} \quad (9)$$

with $q = q_1 + q_2$ and the normalized couplings c_X^V for $(V = \gamma, Z)$ expressed as

$$c^{\gamma}_{\chi^-_H} = c^{\gamma}_{\tilde{\ell}^-_L} = 1, \qquad c^{Z}_{\chi^-_H} = c^{Z}_{\tilde{\ell}^-_L} = \frac{(1/2 - s_W^2)}{c_W s_W},$$
$$c^{Z}_{\chi^0_H} = c^{Z}_{\tilde{\nu}_\ell} = -\frac{1}{2c_W s_W} \tag{10}$$

$$c^{\gamma}_{\chi^-_W} = 1, \qquad c^{Z}_{\chi^-_W} = \frac{c_W}{s_W}, \qquad c^{Z}_{\chi^0_W} = 0 \tag{11}$$

in terms of c_W and s_W.

In addition to the standard three-point vertices in Eqs. (10) and (11), there exists a four-point momentum-independent vertex contributing to the FSR process $V^* \to \gamma\tilde{\ell}^-_L\tilde{\ell}^+_L$ in the L_0 scenario:

$$\langle \gamma^\nu \tilde{\ell}^+_L \tilde{\ell}^-_L || V^\mu \rangle = 2e^2 d^V_{\tilde{\ell}^-_L} g^{\mu\nu} \tag{12}$$

with the normalized couplings $d^{\gamma,Z}_{\tilde{\ell}^-_L}$ identical to $c^{\gamma,Z}_{\tilde{\ell}^-_L}$ given in Eq. (10).

E. Radiatively induced mass difference

Although in all the three scenarios the charged and neutral SUSY particles are degenerate in mass before EWSB, the gauge symmetry-breaking part in the MSSM causes a finite calculable mass splitting through radiative corrections. Moreover, the so-called D-term potential leads to an additional mass splitting between the spin-0 charged slepton and neutral sneutrino in the L_0 scenario unless the two Higgs vacuum expectation values, $v_u = v\cos\beta$ and $v_d = v\sin\beta$, are equal, i.e. $\tan\beta = 1$.

At the leading order, the mass splitting stems from one-loop virtual photon and Z-boson exchange corrections to the masses and the wave functions of the chargino and neutralino states in the $H_{1/2}$ or $W_{1/2}$ scenario [24,29–35,60]. The one-loop mass splitting for the on-shell SUSY states is

$$\Delta m_H = m_{\chi^\pm_H} - m_{\chi^0_H} = \frac{\alpha}{4\pi}\mu[f(m_Z/\mu) - f(0)] \tag{13}$$

$$\Delta m_W = m_{\chi^\pm_W} - m_{\chi^0_W} = \frac{\alpha}{4\pi s_W^2} M_2[f(m_W/M_2) - c_W^2 f(m_Z/M_2) - s_W^2 f(0)], \tag{14}$$

respectively, where the loop function $f(a) = 2\int_0^1 dx(1+x)\ln[x^2 + (1-x)a^2]$ and $\alpha = e^2/4\pi$. The asymptotic value of the mass splitting for $\mu, M_2 \gg m_Z$ is $\alpha m_Z/2 \simeq 355$ MeV and $\alpha m_W/2(1+c_W) \simeq 165$ MeV, respectively. (For the radiatively induced mass splitting to be dominant, the winos/Higgsinos must be separated from the next-heaviest electroweak states. For the $W_{1/2}$ scenario, it suffices that M_1 and μ parameters are of order 1 TeV. In contrast, for the $H_{1/2}$ scenario, the gaugino masses M_1 and M_2 must be above 10 TeV, unless there occur some cancellations between wino and bino contributions [27,61].)

In the L_0 scenario, the charged slepton is in general nondegenerate with the neutral sneutrino, the $SU(2)_L$-doublet partner, due to the D-term contribution leading to a mass splitting of $O(m_Z^2/M_s)$ where M_s is a common SUSY-breaking slepton mass parameter, unless $\tan\beta = 1$. Even if they are degenerate with $\tan\beta = 1$ at the tree level, a leading-order mass splitting arises from one-loop corrections with virtual sleptons of the same and different flavor and Higgs bosons as well as virtual photon, Z-boson and W-boson diagrams. Nevertheless, as the splitting must vanish without EWSB, it is therefore bounded by a quantity proportional to the EM fine structure constant times the Z-boson mass.

III. SINGLE-PHOTON PROCESSES AT e^+e^- COLLIDERS

In the above scenarios, the pair of SUSY states may be produced at the ILC via s-channel γ/Z exchanges. However, as the mass splitting between the charged and neutral states is of the order of a few hundred MeV, the expected signatures at the ILC can vary from soft ($p_T \sim 300$ MeV) decay products through displaced vertices to massive charged tracks. We do not perform any sophisticated analyses for distinguishing the charged modes from the neutral modes in the present work and assume the charged and neutral states in each scenario to be (nearly) degenerate in the following numerical analyses. For more dedicated studies for separating the charged modes from the neutral modes and measuring the mass splitting based on the visible decay products of the charged states, we refer to Refs. [26,27].

One method to search for the production of invisible particles is to identify an associated hard radiated photon in single-photon processes in e^+e^- collisions, $e^+e^- \to \gamma + E$. In the three $\{H_{1/2}, W_{1/2}, L_0\}$ scenarios, a pair of charged or neutral particles, $X\bar{X}$, is produced through a virtual γ or Z-exchange and accompanied by a hard photon radiation in the single-photon process

$$e^+e^- \to \gamma V^* \quad \text{or} \quad V^* \to \gamma X\bar{X} \quad \text{with} \quad V = \gamma, Z. \tag{15}$$

For the neutral $\chi^0_H\chi^0_H$ and $\tilde{\nu}_\ell\tilde{\nu}^*_\ell$ pairs, the photon in the single-photon process (15) is radiated only from the initial electron or positron line, but for every charged pair, the photon is emitted also from the final charged particle lines as shown in Fig. 1. In each process, the ISR and FSR parts are separately EM gauge invariant and develop no interference terms between them (when the Z-boson width is ignored).

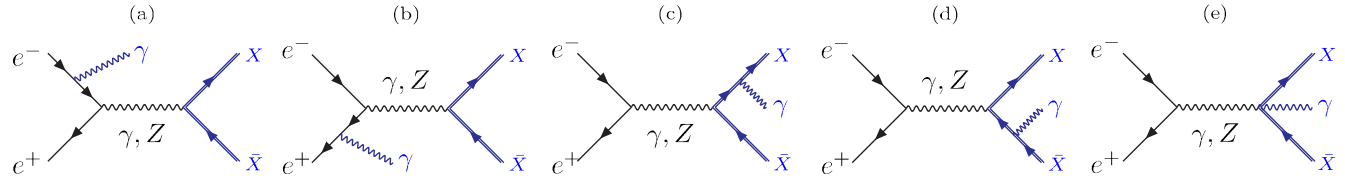

FIG. 1 (color online). Feynman diagrams for the single-photon process $e^+e^- \to \gamma X\bar{X}$ with the charged or neutral particle-antiparticle pair, X and $\bar{X}$. The diagrams (a) and (b) are for the ISR processes with the photons radiated from the initial electron and positron lines with $X = \{\chi^-_{H,W}, \chi^0_H, \tilde{\ell}^-_L, \tilde{\nu}_\ell\}$ and the diagrams (c) and (d) for the FSR processes with the photons emitted from the final-state charged particles with $X = \{\chi^-_{H,W}, \tilde{\ell}^-_L\}$. The diagram (e) involving a four-point coupling is only for a scalar particle $X = \tilde{\ell}^-_L$.

The FSR part has been ignored in most of the previous studies on the single-photon processes. In the present analysis, we include not only the ISR part but also the FSR part for assessing the validity of the ISR approximation and the influence of the FSR part in characterizing the (nearly) invisible particles through single-photon processes in e^+e^- collisions.

A. Initial-state radiation

We ignore the electron mass except for avoiding collinear singularity. We include the possible $e^\pm$ beam polarizations $P_\pm$ in studying the dependence of the signal process $e^+e^- \to \gamma X\bar{X}$ on the photon energy fraction $x_\gamma = 2E_\gamma/\sqrt{s}$ and the photon scattering angle θ_γ with respect to the e^- momentum direction in the e^+e^- c.m. frame.

The ISR effect can be expressed in a factorized form with a universal Weizsacker–Williams radiator function [62–64] as

$$\frac{d\sigma(e^+e^- \to \gamma X\bar{X})_{\rm ISR}}{dx_\gamma d\cos\theta_\gamma} = \mathcal{R}(s; x_\gamma, \cos\theta_\gamma) \times \sigma^{X\bar{X}}(q^2), \quad (16)$$

where the ISR radiator function $\mathcal{R}$ can be expressed to a very good approximation as

$$\mathcal{R}(s; x_\gamma, \cos\theta_\gamma) = \frac{\alpha}{\pi}\frac{1}{x_\gamma}\left[\frac{1+(1-x_\gamma)^2}{1+4m_e^2/s-\cos^2\theta_\gamma} - \frac{x_\gamma^2}{2}\right] \quad (17)$$

which is nearly independent of the beam energy except for the forward or backward collinear direction. The total cross section of the $X\bar{X}$ pair production in e^+e^- annihilation to be evaluated with the reduced c.m. energy squared $q^2 = (1-x_\gamma)s$ is given by

$$\sigma^{X\bar{X}}(q^2) = \frac{2\pi\alpha^2}{3q^2}\beta_q \mathcal{P}(X; P_-, P_+; q^2)\mathcal{K}(\beta_q) \quad (18)$$

with $\beta_q = \sqrt{1-4m_X^2/(1-x_\gamma)s}$, the speed of the particle X in the $X\bar{X}$ c.m. frame. The polarization-dependent factor $\mathcal{P}$ is defined in terms of the beam polarizations and γ and Z-boson propagators as

$$\mathcal{P}(X; P_-, P_+; q^2) = \frac{(1+P_-)(1-P_+)}{4}\left|c_X^\gamma + c_R c_X^Z \frac{q^2}{q^2-m_Z^2}\right|^2 + \frac{(1-P_-)(1+P_+)}{4}\left|c_X^\gamma + c_L c_X^Z \frac{q^2}{q^2-m_Z^2}\right|^2 \quad (19)$$

with $c_L = (1/2 - s_W^2)/c_W s_W$ and $c_R = -s_W/c_W$ and the couplings c_X^γ and c_X^Z given in Eqs. (10) and (11). The kinematical factor $\mathcal{K}(\beta_q)$ reads

$$\mathcal{K}(\beta_q) = \begin{cases} \beta_q^2 & \text{for spin-0 charged slepton or sneutrino} \\ 2(3-\beta_q^2) & \text{for spin-1/2 chargino or neutralino.} \end{cases} \quad (20)$$

The range of x_γ is $0 \le x_\gamma \le 1 - 4m_X^2/s$ with its maximal value $x_\gamma^{\rm max} = 1 - 4m_X^2/s$ corresponding to the $X\bar{X}$ production threshold with $\beta_q = 0$. Asymptotically when $\beta_q \to 0$, i.e. $x_\gamma \to 1 - 4m_X^2/s$, the cross section is proportional to β_q^3 for the spin-0 particles, exhibiting a slowly rising P-wave threshold excitation, but it is proportional to β_q for the spin-1/2 particles, exhibiting a steeply rising S-wave excitation near the threshold.

B. Final-state radiation

Unlike the ISR effect, the FSR parts of the photon-energy and angular distributions are not universal and have no collinear singular term.

For any charged pair $X\bar{X} = \chi^-_H\chi^+_H$, $\chi^-_W\chi^+_W$, $\tilde{\ell}^-_L\tilde{\ell}^+_L$, the dependence of the FSR part on the FSR photon energy fraction x_γ and the photon scattering angle θ_γ can be decomposed as

$$\frac{d\sigma(e^+e^- \to \gamma X\bar{X})_{\rm FSR}}{dx_\gamma d\cos\theta_\gamma} = \frac{3}{8}[(1+\cos^2\theta_\gamma)\mathcal{F}_1^X(s; x_\gamma) + (1-3\cos^2\theta_\gamma)\mathcal{F}_2^X(s; x_\gamma)]\sigma^{X\bar{X}}(s), \quad (21)$$

where the final-state radiator functions $\mathcal{F}_{1,2}^X$ are process dependent. Explicitly, for the production of a chargino pair with $X = \chi^-_H$ or χ^-_W, the FSR radiator functions are given by

$$\mathcal{F}_1^X(s;x_\gamma)=\frac{\alpha}{\pi}\frac{1}{x_\gamma}\frac{\beta_q}{\beta_s}\left[(1+\beta_s^2-2x_\gamma)L(\beta_q)-2(1-x_\gamma)+\frac{2x_\gamma^2}{3-\beta_s^2}[L(\beta_q)-1]\right] \quad (22)$$

$$\mathcal{F}_2^X(s;x_\gamma)=\frac{\alpha}{\pi}\frac{1}{x_\gamma}\frac{\beta_q}{\beta_s}\frac{2}{3-\beta_s^2}[2-2x_\gamma-(1-\beta_s^2)L(\beta_q)] \quad (23)$$

in terms of x_γ with $\beta_s=\sqrt{1-4m_X^2/s}$, the c.m. speed of the X in the process $e^+e^-\to X\bar{X}$ with no photon emission [65]. On the other hand, for the production of a charged slepton pair with $X=\tilde{\ell}_L^-$, the FSR radiator functions read

$$\mathcal{F}_1^X(s;x_\gamma)=\frac{\alpha}{\pi}\frac{1}{x_\gamma}\frac{\beta_q}{\beta_s}\left[(1+\beta_s^2-2x_\gamma)L(\beta_q)-2(1-x_\gamma)+\frac{2x_\gamma^2}{\beta_s^2}\right] \quad (24)$$

$$\mathcal{F}_2^X(s;x_\gamma)=\frac{\alpha}{\pi}\frac{1}{x_\gamma}\frac{\beta_q}{\beta_s}\frac{1}{\beta_s^2}[(3-\beta_s^2-2x_\gamma)L(\beta_q)-6(1-x_\gamma)] \quad (25)$$

with the logarithmic function $L(\beta_q)$ defined by

$$L(\beta_q)=\frac{1}{\beta_q}\ln\left(\frac{1+\beta_q}{1-\beta_q}\right). \quad (26)$$

Integrating the distribution over the full range of the photon scattering angle, the normalized FSR-photon energy distribution approaches a well-known universal FSR radiator function in the soft-photon limit with x_γ close to zero,

$$\mathcal{F}_1^X(s;x_\gamma)\to\frac{\alpha}{\pi}\frac{1}{x_\gamma}[(1+\beta_s^2)L(\beta_s)-2] \quad \text{as} \quad x_\gamma\to 0, \quad (27)$$

independently of the spin of the charged particle emitting the photon [66,67].

When the photon energy fraction approaches the $X\bar{X}$ threshold, the radiator function $\mathcal{F}_2^X$ goes to zero $\sim\beta_q^3$ for both the spin-0 and spin-1/2 cases. In contrast to this P-wave behavior, the radiator function $\mathcal{F}_1^X$ exhibits an S-wave threshold behavior as

$$\mathcal{F}_1^X(s;x_\gamma)\to\frac{\alpha}{\pi}\beta_q\begin{cases}2/\beta_s & \text{for spin-0 charged slepton}\\ 2\beta_s/(3-\beta_s^2) & \text{for spin-1/2 chargino}\end{cases} \quad \text{as} \quad x_\gamma\to\beta_s^2 \quad (28)$$

not only for the spin-1/2 chargino case but also for the spin-0 charged slepton case. In the charged slepton case, the S-wave excitation of the FSR part is due to the momentum-independent four-point contact terms contributing to the diagram in Fig. 1(e).

C. Effects of the ISR and FSR in charged pair production

The FSR part in the photon-associated charged pair production is expected to be much smaller in magnitude than the ISR part as the photon in the FSR part is generated from a charged particle much heavier than the electron. Because of this generally expected feature, the FSR part has been ignored in most previous analytic and numerical analyses on the single-photon processes. In this subsection, we assess the validity of the ISR approximation critically by exploiting the ratio of the FSR part to the ISR part defined as

$$\mathcal{R}_{\rm FI}(x_\gamma)=\frac{d\sigma(e^+e^-\to\gamma X\bar{X})_{\rm FSR}/dx_\gamma}{d\sigma(e^+e^-\to\gamma X\bar{X})_{\rm ISR}/dx_\gamma} \quad (29)$$

in terms of the x_γ-dependent distributions derived by integrating Eqs. (16) and (21) over the scattering angle θ_γ, respectively.

Figure 2 shows the dependence of the ratio of the FSR part to the ISR part for two mass values, $m_X=100$ (solid lines) and 200 GeV (dashed lines). The photon scattering

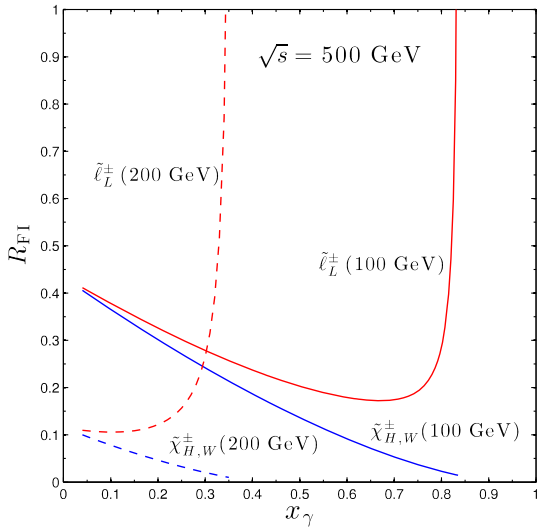

FIG. 2 (color online). Ratio of the FSR to the ISR vs x_γ in the production of a charged pair at a 500 GeV ILC. The solid and dashed lines are for $m_X=100$ and 200 GeV, respectively. The upward (red) and falling (blue) lines are for the spin-0 charged slepton case and the spin-1/2 chargino case, respectively.

angle has been restricted to $10° < \theta_\gamma < 170°$. As the falling (blue) lines indicate, the FSR part of the chargino pair production cross section is consistently smaller than the corresponding ISR part, and it becomes negligible, in particular, near the threshold. As the mass increases, the ratio is even more suppressed. Nevertheless, for more precise mass and coupling measurements, it will be more meaningful to include the FSR part in any realistic analyses.

In contrast to the spin-1/2 chargino case, the ratio of the FSR part to the ISR part does not monotonically decrease with increasing x_γ in the slepton scenario. In fact, the ratio blows up near the threshold, as the FSR part decreases in proportion to β_q in S-waves while the ISR part decreases in proportion to β_q^3 in P-waves. Therefore, the FSR contribution qualitatively changes the threshold behavior, although it would be challenging to quantitatively determine the fast-falling distribution at the threshold with limited statistics, as will be discussed in Sec. IV B.

IV. CHARACTERISTICS OF THE PRODUCTION CROSS SECTIONS

The most severe irreducible background to the signal events under consideration is the standard $e^+e^- \to \gamma\nu\bar{\nu}$ with $\nu = \nu_e$, ν_μ and ν_τ. For the sake of comparison, the unpolarized x_γ distribution for the background is shown (solid line on the top) together with the distributions for different SUSY EW particles with $m_X = 100$ GeV in Fig. 3. Throughout this paper, we will illustrate our results for a 500 GeV ILC.

For $m_X > m_Z/2$, one powerful kinematic cut for reducing the irreducible background reaction $e^+e^- \to \gamma\nu\bar{\nu}$ can be

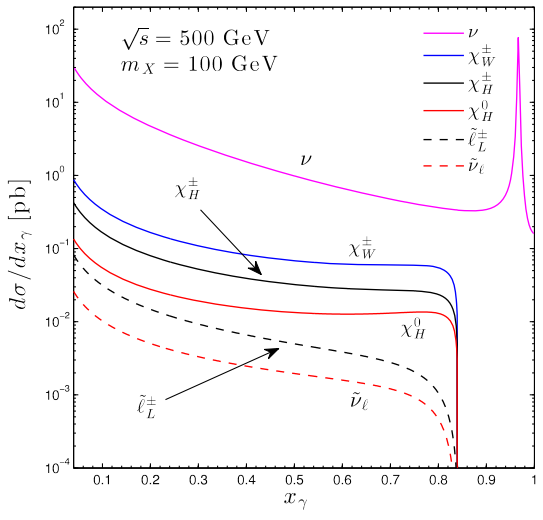

FIG. 3 (color online). Unpolarized x_γ distribution $d\sigma/dx_\gamma$ with $m_X = 100$ GeV at a 500 GeV ILC, for different SUSY EW particles, as well as that of the background process $e^+e^- \to \gamma\nu\bar{\nu}$ (solid line on the top). The photon scattering angle has been restricted to $10° < \theta_\gamma < 170°$.

applied to the recoil mass squared $q^2 = (q_1 + q_2)^2 = (p_1 + p_2 - k)^2 = s(1 - x_\gamma)$ which can be very accurately reconstructed by measuring the photon energy fraction x_γ. We evaluate the overall statistical significance $N_{\rm SD}$ for the signal and background by summing over all events not only with the photon energy and angular cuts applied but also with the recoil mass cut $\sqrt{q^2} > 2m_X$. Note that this mass cut eliminates the Z-pole contribution to the $\gamma\nu\bar{\nu}$ background.

Another way of removing the background significantly is to exploit the electron and positron beam polarizations. The t-channel W-exchange diagrams contribute to the background process $e^+e^- \to \gamma\nu_e\bar{\nu}_e$ only for the left-handed electrons so that the background can be significantly reduced by taking the right-handed electron and left-handed positron beams. However, which beam polarization is more efficient for the signal significance is determined also according to the polarization dependence of the signal events.

A. Statistical significance of signal events

To quantify whether an excess of signal photons from the $X\bar{X}$ pair production, $N_S = \mathcal{L}\sigma$ for a given integrated luminosity $\mathcal{L}$, can be measured over the $N_B = \mathcal{L}\sigma_B$ SM background photons from the radiative neutrino production, we define a simple-minded theoretical significance

$$N_{\rm SD} = \frac{N_S}{\sqrt{N_S + N_B}} = \frac{\sigma}{\sqrt{\sigma + \sigma_B}}\sqrt{\mathcal{L}}. \qquad (30)$$

For our simple numerical analysis, we require the photon energy to be $E_\gamma > 10$ GeV, corresponding to $x_\gamma > 0.04$, and the photon scattering angle to be $10° < \theta_\gamma < 170°$ so as to guarantee that the photon will have an accurate momentum measurement. We also assume the c.m. energy $\sqrt{s} = 500$ GeV and the total integrated luminosity $\mathcal{L} = 0.5$ ab^{-1}.

The number of signal events needed for a required $N_{\rm SD}$ depends not only on the beam polarization but also on m_X, since the recoil mass cut $\sqrt{q^2} = 2m_X$ is applied to the background process. For example, for $m_X = 100$ GeV, the total cross section of the background for $(P_-, P_+) = (-0.8, +0.3)$ is about 6230 fb implying $N_S \sim 8840$ signal events needed for statistical significance $N_{\rm SD} = 5$, while for $(P_-, P_+) = (+0.8, -0.3)$ the cross section is 400 fb, and only $N_S \sim 2250$ signal events is enough to reach $N_{\rm SD} = 5$.

Figure 4 shows the dependence of the signal significance $N_{\rm SD}$ on the mass m_X. The left panel is for the spin-1/2 chargino or neutralino pair production, and the right panel is for the spin-0 slepton pair production. In each panel, the solid lines are for the left-handed electron and right-handed positron beam polarizations with $(P_-, P_+) = (-0.8, +0.3)$, and the dashed lines are for the right-handed electron and left-handed positron beam polarization with $(P_-, P_+) = (+0.8, -0.3)$.

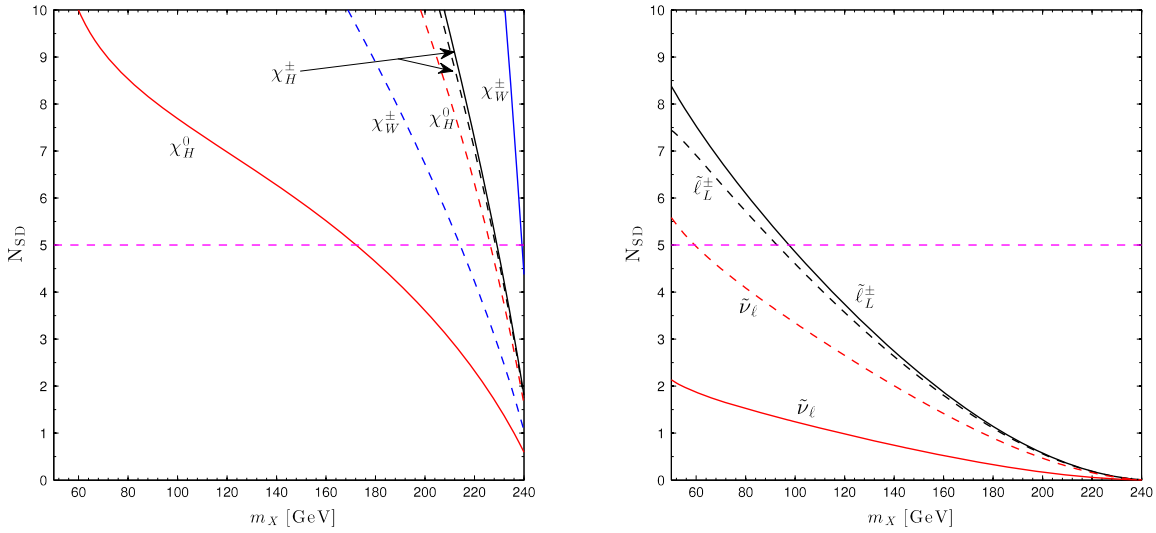

FIG. 4 (color online). Statistical significance N_{SD} vs m_X for $\sqrt{s} = 500$ GeV and the total integrated luminosity $\mathcal{L} = 0.5$ ab^{-1}. The left panel is for the spin-1/2 chargino or neutralino pair production and the right panel for the spin-0 slepton pair production. The solid/dashed lines are for the left-handed/right-handed electron and right-handed/left-handed positron beam polarizations with $(P_-, P_+) = (\mp 0.8, \pm 0.3)$, respectively.

The value of the statistical significance N_{SD} is very sensitive to the beam polarizations in the wino-type chargino $\chi_W^\pm$ and Higgsino-type neutralino χ_H^0 cases. As the red solid and dashed lines in the left panel indicate, the significance for the Higgsino-type neutralino χ_H^0 is enhanced with the right-handed/left-handed electron/positron beam polarizations. On the contrary, the significance for the wino-type chargino $\chi_W^\pm$ is greatly enhanced with the left-hand/right-handed electron/positron beam polarizations. In both $H_{1/2}$ and $W_{1/2}$ scenarios, the neutralinos as well as charginos can be discovered with large statistical significances up to their mass close to the beam energy $\sqrt{s}/2$.

In contrast, as shown in the right panel of Fig. 4, the value of the statistical significance for the charged slepton pair and the sneutrino pair production is so small that the charged slepton and the neutral sneutrino can be discovered only when its mass is less than ~100 and 60 GeV, respectively. Higher integrated luminosity would thus be desirable for the scalar state searches.

B. Spin determination

As indicated by the kinematical factor $\mathcal{K}(\beta_q)$ in Eq. (20), the threshold behavior of the production cross section of a neutral pair is distinctly different in the spin-0 and spin-1/2 cases. As the red solid and dashed lines in Fig. 5 show, the normalized cross section for a spin-1/2 Higgsino-type Dirac neutralino pair is steeply excited in S-waves at the threshold, but the corresponding cross section for a spin-0 sneutrino pair is slowly excited in P-waves. In this neutral pair production case, the spin identification can be made unambiguously through the x_γ distribution pattern near the threshold.

Like the neutral case, the ISR part of the production cross section for a charged pair exhibits an S-wave and P-wave excitation for the spin-1/2 and spin-0 particles, respectively. As pointed out before, the FSR part is steeply excited in S-waves even in the spin-0 case, which could spoil the characteristic spin-0 P-wave threshold behavior for the ISR part. However, as can be checked quantitatively with the relative contribution of the FSR part in Fig. 2, the FSR part becomes larger than the ISR only when the photon energy fraction x_γ is extremely close to the threshold value, where both the FSR and ISR parts are already very small due to the suppressed phase-space factor β_q. Therefore, as shown

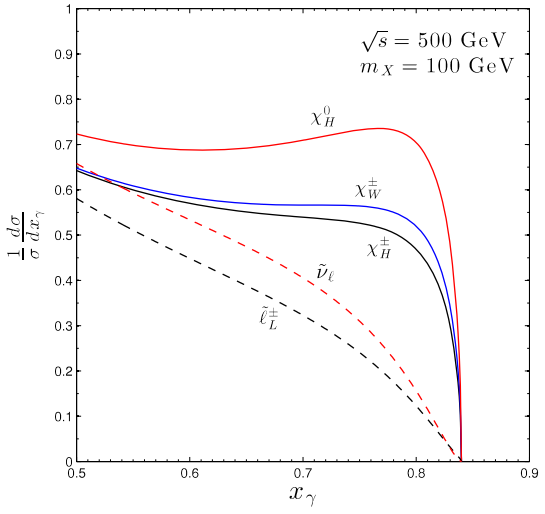

FIG. 5 (color online). Normalized distribution vs the photon energy fraction x_γ with $m_X = 100$ GeV. Effects of both FSR and ISR are included.

in Fig. 5, the spin of the SUSY EW particles can be determined through the excitation pattern of the (normalized) photon energy distributions near the threshold—a sharp S-wave excitation for a spin-1/2 particle and a slow P-wave excitation for a spin-0 particle, only with a negligible contamination of the FSR part even for the charged pair production.

It would be instructive to quantify the statistical significance of the measurement for the energy distributions. Assuming the c.m. energy $\sqrt{s} = 500$ GeV and the total integrated luminosity $\mathcal{L} = 0.5$ ab^{-1}, we examine the signal distributions after the background subtraction, like those in Fig. 5. For illustration, we compare the three production scenarios for $H_{1/2}$, $W_{1/2}$ and L_0. In Figs. 6, we show predicted shapes of the event distributions vs x_γ by the solid curves, for $m_X = 100$ (upper row) and 60 GeV (lower row), respectively. To be realistic, we also include the statistical error bars as determined by the large number of background events $\sqrt{N_B}$ in the last three bins near the threshold. As noticed earlier, the $L_{1/2}$ scalar signal is not nearly as good as the fermionic states. Thus, the spectrum determination near the threshold is significantly worse as shown in Figs. 6(c) and 6(f). Nevertheless, the difference between the spin-1/2 and spin-0 distributions is unambiguously distinguishable as seen from the figures. The difference becomes more distinctive for lighter states. If future data hint at a low cross section scalar signal, it will warrant a dedicated experimental study including soft decay products, which could significantly improve signal-to-background ratio as shown in Ref. [27]. In such a case, a definitive confirmation of the scalar nature could be achieved already with moderate luminosities.

C. Ratio of left-handed and right-handed cross sections

To see the polarization dependence of the signal cross sections, we define the left-right (LR) ratio of the purely right-handed cross section to the purely left-handed cross section,

$$\mathcal{R}_{\rm LR}(X; x_\gamma) = \frac{d\sigma(e^+e^-_R \to \gamma X\bar{X})/dx_\gamma}{d\sigma(e^+e^-_L \to \gamma X\bar{X})/dx_\gamma}, \qquad (31)$$

obtained after applying the photon-angle cut described before. Figure 7 shows the x_γ dependence of the ratio of the right-handed electron cross section to the left-handed electron cross section.

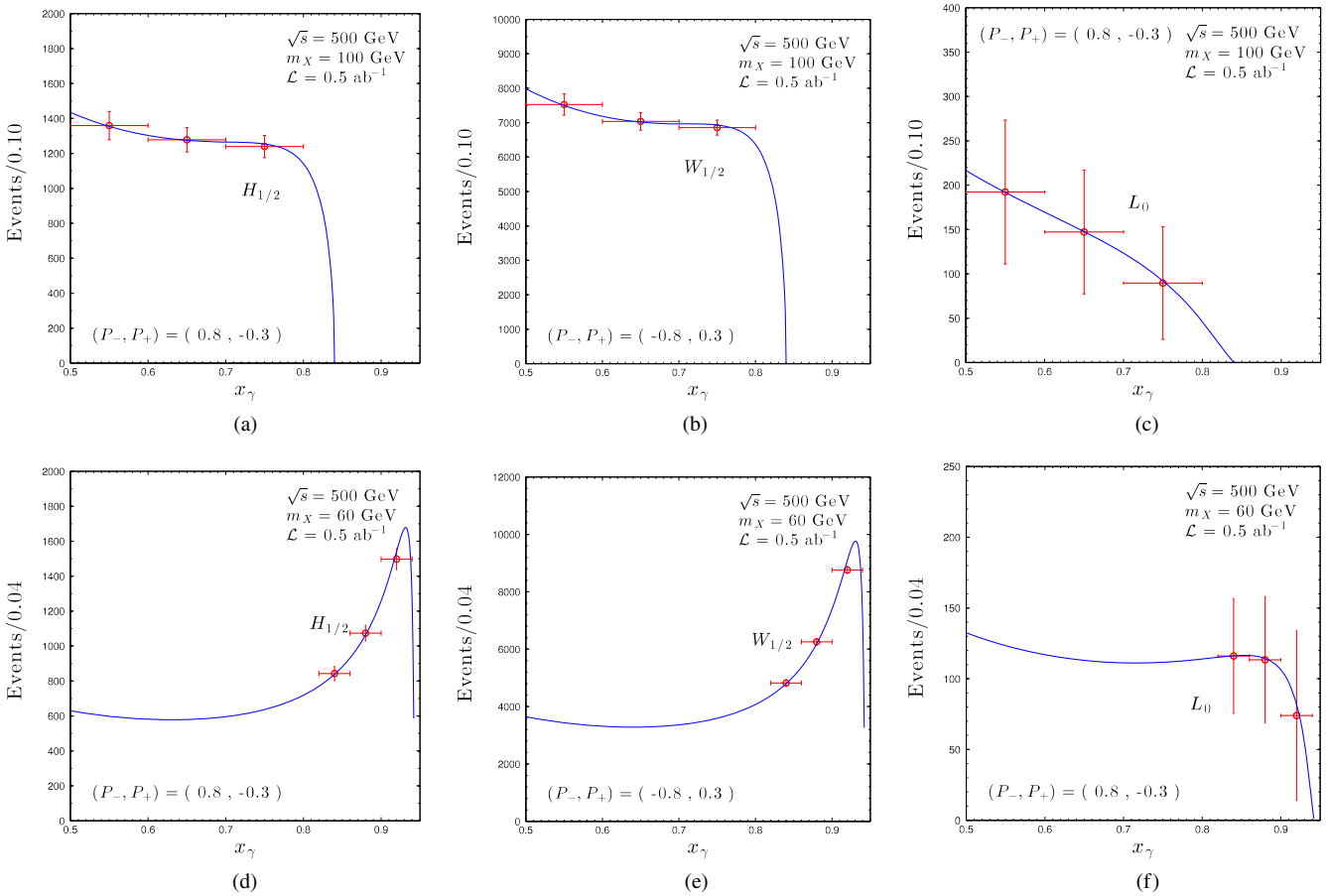

FIG. 6 (color online). Photon energy fraction distribution near the threshold, after the background subtraction, with $m_X = 100$ (first row) and 60 GeV (second row). The three statistical error bars in each panel correspond to the background fluctuation $\sqrt{N_B}$.

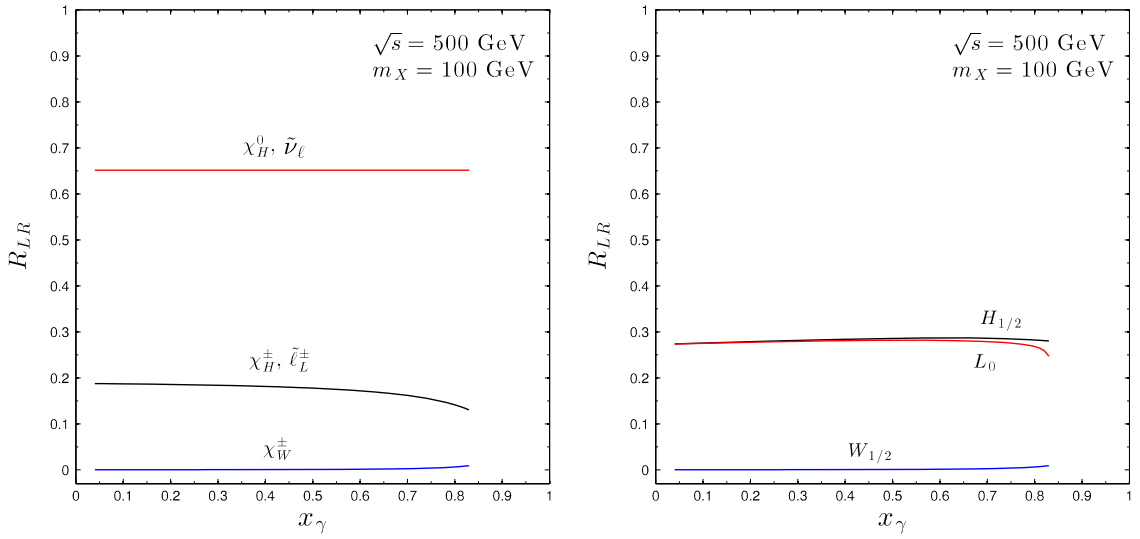

FIG. 7 (color online). Ratio of the purely right-handed electron cross section to the purely left-handed electron cross section vs the photon energy fraction x_γ with $m_X = 100$ GeV. Left panel: individual channels of the pair production. Right panel: inclusive sums of the charged and neutral pair production.

Before discussing the features that the LR ratios exhibit, we note that for $m_X = 100$ GeV the inequality relation $s \geq q^2 \geq 4m_X^2 = 4 \times 10^4$ GeV$^2 \gg m_Z^2$ is satisfied so that the polarization factor $\mathcal{P}$ defined in Eq. (19) is nearly constant over the whole x_γ range [0.05,0.84]. In particular, for the neutral pair production with the photon radiated from the initial electron or positron line and with no virtual-photon exchange, the ratio is indeed constant, and its value for the SU(2)$_L$-doublet state $X = \chi_H^0, \tilde{\nu}_\ell$ is given by

$$\mathcal{R}_{\rm LR}[X] = \frac{c_R^2}{c_L^2} = \frac{s_W^4}{(1/2 - s_W^2)^2} \simeq 0.648 \quad \text{for } X = \chi_D^0, \tilde{\nu}_\ell \tag{32}$$

independently of the spin of the produced particle X for $s_W^2 \simeq 0.223$ given in Ref. [68], as shown in the left frame of Fig. 7.

In contrast to the neutral pair production, the LR ratio for each charged pair production exhibits a slight dependence on the photon energy fraction x_γ with a visible variation near the threshold with $x_\gamma = 1 - 4m_X^2/s = 0.84$ (see the lower two lines in the left frame of Fig. 7). The reason is that the cross section for the charged pair production consists not only of the ISR but also of the FSR parts which have different x_γ-dependent radiator functions as well as slightly different x_γ-dependent polarization factors. Note that the initial polarization factor is a function of q^2, i.e. x_γ, while the final polarization factor is constant for a given $\sqrt{s}$. Neglecting the slight variations due to the FSR contributions, the LR ratio $\mathcal{R}_{\rm LR}$ is given to a good approximation by

$$\mathcal{R}_{\rm LR}[X] \simeq \begin{cases} 4s_W^4 \approx 0.199 & \text{for } X = \chi_H^-, \tilde{\ell}_L^- \\ 0 & \text{for } X = \chi_W^-. \end{cases} \tag{33}$$

The approximately zero ratio $\mathcal{R}_{\rm LR}$ in the wino-type chargino case can be traced to the perfect cancellation between the γ and Z exchange diagrams for the right-handed electron beam polarization, i.e. $1 + c_R c_{\chi_W^-}^Z = 1 - (s_W/c_W)(c_W/s_W) = 0$ in the asymptotic limit.

The right frame of Fig. 7 shows the LR ratio of the inclusive sum of the charged and neutral pair production cross sections in each scenario. Again this inclusive LR ratio remains almost constant and enables us to distinguish the $W_{1/2}$ scenario from the $H_{1/2}$ and L_0 scenarios.

Figure 8 shows the statistical errors of the LR ratio measurements as determined by the background fluctuation $\sqrt{N_B}$, for the three scenarios with two different representative masses $m_X = 100$ (left panel) and 60 GeV (right panel), assuming $\sqrt{s} = 500$ GeV c.m. energy and $\mathcal{L} = 0.5$ ab^{-1} luminosity with both polarizations $(P_-, P_+) = (\mp 0.8, \pm 0.3)$. It is clear that the $W_{1/2}$ and $H_{1/2}$ scenarios show very distinct value, even after the fluctuation of the background is included. However, similar to the spin determination, it is less impressive to measure the ratio for the $L_{1/2}$ scenario, due to its low significance.

D. Alternative discrimination methods

While the Higgsino-type neutralino χ_H^0 in the $H_{1/2}$ scenario is a Dirac fermion, the wino-type neutralino χ_W^0 in the $W_{1/2}$ scenario is a Majorana fermion. Unlike the Dirac neutralino, the Majorana neutralino χ_W^0 can mediate via a t-channel exchange a typical fermion-number violating process such as the same-sign chargino-pair production process, $W^-W^- \to \chi_W^- \chi_W^-$. The possible e^-e^- collision mode of the ILC experiments enables us to distinguish the $W_{1/2}$ scenario from the $H_{1/2}$ scenario by searching for

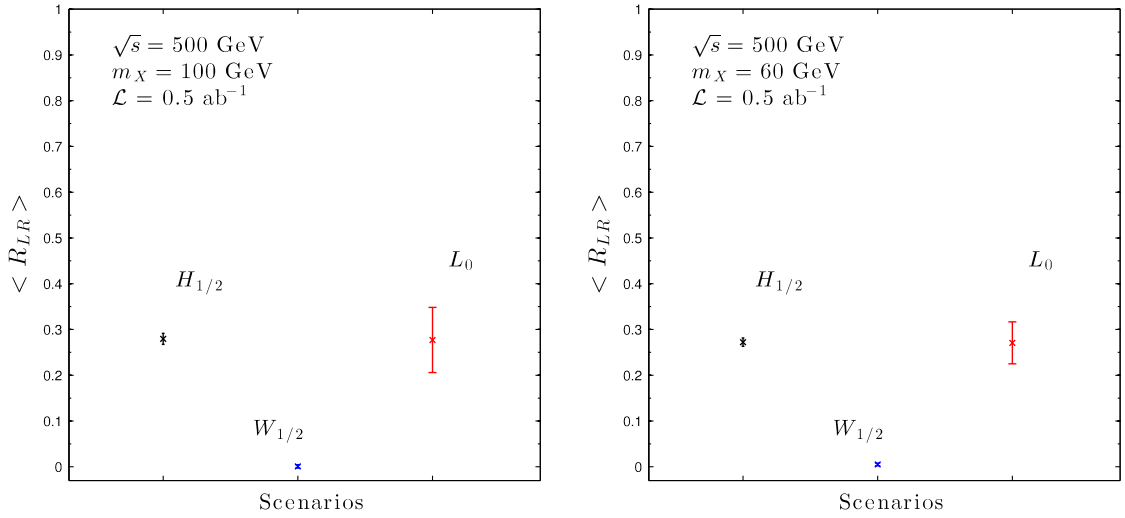

FIG. 8 (color online). Ratio of the purely right-handed electron total cross section to the purely left-handed electron total cross section vs the photon energy fraction x_γ with $m_X = 100$ (left panel) and 60 GeV (right panel). The statistical error bars correspond to the background fluctuation $\sqrt{N_B}$ that comes from the measurement of the total cross sections with polarizations $(P_-, P_+) = (\mp 0.8, \pm 0.3)$.

the same-sign WW fusion process via the process $e^-e^- \to \nu_e\nu_e W^-W^- \to \nu_e\nu_e \bar{\chi}_W^- \bar{\chi}_W^-$.

Although the neutral state X^0 of the (nearly) degenerate pair $[X^-, X^0]$ in each scenario is stable, the charged state X^- can decay to X^0 via charged current interactions. For the typical loop-induced mass differences of a few hundred MeV, the most important decay modes are $X^- \to X^0\pi^-$, $X^0 e^- \bar{\nu}_e$ and $X^0\mu^-\bar{\nu}_\mu$. The decay products typically have low p_T, but as demonstrated for the proposed International Large Detector (ILD) at the ILC, a tracking efficiency of 60% can be expected down to p_T values of 200 MeV [38]. On the other hand, the inner layer of the ILD vertex detector would be extended down to the radius of 1.6 cm, therefore offering good prospects of observing X^- tracks, which in this case would have a decay length of $\mathcal{O}(10$ cm$)$ or less. The combination of different detection methods based on the massive charged tracks, displaced vertices and soft decay products will enable us to cover all mass differences. Since relatively low data volumes are expected, no hardware trigger would be needed allowing for the search of rare processes. Even in the case when the decays products can be observed, all scenarios analyzed here would lead to the same final state. The angular photon distributions would therefore offer a convenient discrimination method. Finally, angular distributions of the decay products would provide additional information on the spin, but such an analysis is beyond scope of the present study.

V. SUMMARY AND CONCLUSIONS

Given the current null results for SUSY searches at the LHC, we were strongly motivated to consider the situation in which the only accessible SUSY states are EW gauginos, Higgsinos or sleptons. We explored three characteristic scenarios, each of which has a nearly degenerate pair of a charged state and a neutral state with a small mass difference. In the framework of the MSSM, the three cases can be characterized as (a) two spin-1/2 Higgsino $\mathrm{SU}(2)_L$ doublets, (b) a spin-1/2 wino $\mathrm{SU}(2)_L$ triplet and (c) a spin-0 left-handed slepton $\mathrm{SU}(2)_L$ doublet beyond the SM particle spectrum. We presented the theoretical structures, their interactions with the SM fields and their radiatively induced mass splitting in Sec. II.

Due to near mass degeneracy, not only the neutral particle but also the charged particle of each pair is not easily detectable in collider experiments. We first presented the analytic expressions for the pair production of an invisible neutral pair involving a hard photon emission and discussed their general features from the initial-state radiation and the final-state radiation in Sec. III. In our numerical studies, we illustrated our results with a 500 GeV ILC. We provided a detailed and systematic analysis with polarized electron and positron polarizations so as to check the detectability of the charged particles as well as neutral particles and how well their properties can be characterized. As discussed in Sec. III C, the FSR effect in the spin-1/2 charged pair production, compared to the ISR part, decreases monotonically in size from about 40% (10%) for $x_\gamma = 0.04$ and becomes negligible close to the threshold with $x_\gamma = 0.84(0.36)$ for $m_X = 100(200)$ GeV and $\sqrt{s} = 500$ GeV. Therefore, the previous analyses in the literature based on the ISR approximation are rather reliable, especially when the mass m_X is not far from the half of the e^+e^- c.m. energy $\sqrt{s}$. On the contrary, in the spin-0 charged pair production, the FSR effect becomes larger than the ISR part near the threshold as shown in Fig. 2, which might endanger any consequences based simply on the ISR approximation. Nevertheless, we found

that, in spite of the FSR contamination, the results based on the ISR approximation are quantitatively very similar to those with both the ISR and FSR parts.

In Sec. IV A, we studied the signal observation with respect to the SM backgrounds. We also demonstrated in Sec. IV B that the excitation pattern near the threshold can be exploited through the photon energy distribution to determine the spin of the SUSY EW particles unambiguously. The (normalized) photon energy distribution near threshold shows a steeply rising S-wave excitation for a spin-$1/2$ pair and a slowly rising P-wave excitation for a spin-0 pair, even after the contamination from the FSR part is included (see Fig. 5). For two representative masses $m_X = 100$ and 60 GeV, we showed, in Fig. 6, that the threshold patterns of the $H_{1/2}$ and $W_{1/2}$ scenarios can be determined with a good accuracy at the ILC with the c.m. energy $\sqrt{s} = 500$ GeV and the total integrated luminosity $\mathcal{L} = 0.5$ ab^{-1}, and they are notably distinctive from the $L_{1/2}$ scenario.

Furthermore, the LR ratio of right-handed and left-handed cross sections introduced in Sec. IV C takes very different values according to the production modes: $\sim s_W^4/(1/2 - s_W^2)^2 \simeq 0.65$ for $X = \chi_D^0$ and $\tilde{\nu}_\ell$; $\sim 4s_W^4 \simeq 0.20$ for $X = \chi_H^-$ and $\tilde{\ell}_L^-$; ~ 0 for $X = \chi_W^-$. Even after taking the inclusive sum of the charged and neutral modes in each scenario, the LR ratio has a nearly constant value that can be used for distinguishing the $W_{1/2}$ scenario from the others even with statistical error included, as shown in Figs. 7 and 8. Therefore, in addition to enhancing the statistical significance sizably, the electron and positron beam polarizations are very powerful in characterizing the production modes. Combining the LR ratio and the threshold excitation pattern, we can identify unambiguously which scenario among the three scenarios is realized. Our analyses are easily generalizable to other collider energies as long as the pair production is kinematically accessible.

Our analytic and numerical results demonstrate clearly the strong physics potential of the ILC in detecting and characterizing the invisible particles, complementary to the very difficult searching environment at the LHC. Further detailed analyses and detector simulations may be needed to reach fully realistic conclusions at the ILC.

ACKNOWLEDGMENTS

The work of S. Y. C. was supported in part by Basic Science Research Program through the National Research Foundation funded by the Ministry of Education, Science and Technology (Grant No. NRF-2011-0010835) and in part by research funds of Chonbuk National University in 2013. T. H. and X. W. were supported in part by the U.S. Department of Energy under Grant No. DE-FG02-95ER40896, in part by the PITT PACC. Work was partially supported by the Polish National Science Centre under research Grants No. DEC-2012/05/B/ST2/02597 and No. OPUS-2012/05/B/ST2/03306. K. R. has been partially supported by the MINECO, Spain, under Contract No. FPA2013-44773-P; Consolider-Ingenio CPAN Grant No. CSD2007-00042; Spanish MINECO Centro de Excelencia Severo Ochoa Program under Grant No. SEV-2012-0249 and by JAE-Doc program.

[1] G. Aad *et al.* (ATLAS Collaboration), Phys. Lett. B **716**, 1 (2012).
[2] S. Chatrchyan *et al.* (CMS Collaboration), Phys. Lett. B **716**, 30 (2012).
[3] M. Duehrssen, ATLAS and CMS Collaborations, Moriond, 2015 (unpublished), https://indico.in2p3.fr/event/10819/session/3/contribution/102/material/slides/1.pdf.
[4] F. Caola and K. Melnikov, Phys. Rev. D **88**, 054024 (2013).
[5] V. Khachatryan *et al.* (CMS Collaboration), Phys. Lett. B **736**, 64 (2014).
[6] K. G. Wilson, Phys. Rev. D **3**, 1818 (1971).
[7] E. Gildener, Phys. Rev. D **14**, 1667 (1976).
[8] S. Weinberg, Phys. Lett. B **82**, 387 (1979).
[9] G. 't Hooft, NATO Sci. Ser. B **59**, 135 (1980).
[10] H. P. Nilles, Phys. Rep. **110**, 1 (1984).
[11] H. E. Haber and G. L. Kane, Phys. Rep. **117**, 75 (1985).
[12] K. Griest and M. Kamionkowski, Phys. Rep. **333–334**, 167 (2000).
[13] For a recent review on particle dark matter, see e. g. G. Bertone, D. Hooper, and J. Silk, Phys. Rep. **405**, 279 (2005).
[14] G. F. Giudice and A. Romanino, Nucl. Phys. **B699**, 65 (2004); **B706**, 487(E) (2005).
[15] N. Arkani-Hamed, S. Dimopoulos, G. F. Giudice, and A. Romanino, Nucl. Phys. **B709**, 3 (2005).
[16] J. D. Wells, Phys. Rev. D **71**, 015013 (2005).
[17] H. Baer, V. Barger, P. Huang, and X. Tata, J. High Energy Phys. 05 (2012) 109.
[18] M. Papucci, J. T. Ruderman, and A. Weiler, J. High Energy Phys. 09 (2012) 035.
[19] S. Jung and J. D. Wells, Phys. Rev. D **89**, 075004 (2014).
[20] C. H. Chen, M. Drees, and J. F. Gunion, Phys. Rev. Lett. **76**, 2002 (1996).
[21] C. H. Chen, M. Drees, and J. F. Gunion, Phys. Rev. D **55**, 330 (1997); **60**, 039901(E) (1999).
[22] G. F. Giudice, T. Han, K. Wang, and L.-T. Wang, Phys. Rev. D **81**, 115011 (2010).

[23] T. Han, S. Padhi, and S. Su, Phys. Rev. D **88**, 115010 (2013).
[24] K. Cheung, C.-W. Chiang, and J. Song, J. High Energy Phys. 04 (2006) 047.
[25] H. Baer, V. Barger, and P. Huang, J. High Energy Phys. 11 (2011) 031.
[26] C. Hensel, Report No. DESY-THESIS-2002-047.
[27] M. Berggren, F. Brümmer, J. List, G. Moortgat-Pick, T. Robens, K. Rolbiecki, and H. Sert, Eur. Phys. J. C **73**, 2660 (2013).
[28] H.-C. Cheng, B. A. Dobrescu, and K. T. Matchev, Nucl. Phys. **B543**, 47 (1999).
[29] T. Gherghetta, G. F. Giudice, and J. D. Wells, Nucl. Phys. **B559**, 27 (1999).
[30] K. Cheung and C.-W. Chiang, Phys. Rev. D **71**, 095003 (2005).
[31] J. L. Feng, T. Moroi, L. Randall, M. Strassler, and S.-f. Su, Phys. Rev. Lett. **83**, 1731 (1999).
[32] M. Ibe, T. Moroi, and T. T. Yanagida, Phys. Lett. B **644**, 355 (2007).
[33] S. Dimopoulos, N. Tetradis, R. Esmailzadeh, and L. J. Hall, Nucl. Phys. **B349**, 714 (1991); **B357**, 308(E) (1991).
[34] S. D. Thomas and J. D. Wells, Phys. Rev. Lett. **81**, 34 (1998).
[35] M. Sher, Phys. Rev. D **52**, 3136 (1995).
[36] T. Behnke *et al.*, arXiv:1306.6327.
[37] H. Baer *et al.*, arXiv:1306.6352.
[38] T. Behnke *et al.*, arXiv:1306.6329.
[39] S. Chatrchyan *et al.* (CMS Collaboration), J. High Energy Phys. 09 (2012) 094.
[40] G. Aad *et al.* (ATLAS Collaboration), J. High Energy Phys. 04 (2013) 075.
[41] A. Birkedal, K. Matchev, and M. Perelstein, Phys. Rev. D **70**, 077701 (2004).
[42] H. K. Dreiner, M. Huck, M. Krämer, D. Schmeier, and J. Tattersall, Phys. Rev. D **87**, 075015 (2013).
[43] E. Ma and J. Okada, Phys. Rev. Lett. **41**, 287 (1978); **41**, 1759(E) (1978).
[44] K. J. F. Gaemers, R. Gastmans, and F. M. Renard, Phys. Rev. D **19**, 1605 (1979).
[45] G. Barbiellini, B. Richter, and J. Siegrist, Phys. Lett. B **106**, 414 (1981).
[46] D. Fargion, M. Y. Khlopov, R. V. Konoplich, and R. Mignani, Phys. Rev. D **54**, 4684 (1996).
[47] K. Grassie and P. N. Pandita, Phys. Rev. D **30**, 22 (1984).
[48] P. Fayet, Phys. Lett. B **175**, 471 (1986).
[49] D. A. Dicus, S. Nandi, and J. Woodside, Phys. Lett. B **258**, 231 (1991).
[50] J. L. Lopez, D. V. Nanopoulos, and A. Zichichi, Phys. Rev. Lett. **77**, 5168 (1996).
[51] H. K. Dreiner, O. Kittel, and U. Langenfeld, Phys. Rev. D **74**, 115010 (2006).
[52] S. Y. Choi, J. S. Shim, H. S. Song, J. Song, and C. Yu, Phys. Rev. D **60**, 013007 (1999).
[53] R. Basu, P. N. Pandita, and C. Sharma, Phys. Rev. D **77**, 115009 (2008).
[54] P. Konar, K. Kong, K. T. Matchev, and M. Perelstein, New J. Phys. **11**, 105004 (2009).
[55] C. Bartels, M. Berggren, and J. List, Eur. Phys. J. C **72**, 2213 (2012).
[56] P. N. Pandita and M. Patra, Phys. Rev. D **88**, 055018 (2013).
[57] G. V. Borisov, V. N. Larin, and F. F. Tikhonin, Z. Phys. C **41**, 287 (1988).
[58] K. J. Abraham, J. Kalinowski, and P. Sciepko, Phys. Lett. B **339**, 136 (1994).
[59] D. Choudhury, J. Kalinowski, and A. Kulesza, Phys. Lett. B **457**, 193 (1999).
[60] D. M. Pierce, J. A. Bagger, K. T. Matchev, and R.-j. Zhang, Nucl. Phys. **B491**, 3 (1997).
[61] G. D. Kribs, A. Martin, and T. S. Roy, J. High Energy Phys. 01 (2009) 023.
[62] O. Nicrosini and L. Trentadue, Phys. Lett. B **231**, 487 (1989).
[63] G. Montagna, O. Nicrosini, F. Piccinini, and L. Trentadue, Nucl. Phys. **B452**, 161 (1995).
[64] F. A. Berends and R. Kleiss, Nucl. Phys. **B260**, 32 (1985).
[65] Y. L. Dokshitzer, V. A. Khoze, and W. J. Stirling, Nucl. Phys. **B428**, 3 (1994).
[66] F. E. Low, Phys. Rev. **110**, 974 (1958).
[67] T. H. Burnett and N. M. Kroll, Phys. Rev. Lett. **20**, 86 (1968).
[68] K. A. Olive *et al.* (Particle Data Group Collaboration), Chin. Phys. C **38**, 090001 (2014).